A Recurrent *De Novo* Heterozygous COG4 Substitution Leads to Saul-Wilson Syndrome, Disrupted Vesicular Trafficking, and Altered Proteoglycan Glycosylation

Carlos R. Ferreira,[1,2,29,*] Zhi-Jie Xia,[3,29] Aurélie Clément,[4,29] David A. Parry,[5,29] Mariska Davids,[6,29] Fulya Taylan,[7,29] Prashant Sharma,[6] Coleman T. Turgeon,[8] Bernardo Blanco-Sánchez,[4] Bobby G. Ng,[3] Clare V. Logan,[5] Lynne A. Wolfe,[6] Benjamin D. Solomon,[9] Megan T. Cho,[9] Ganka Douglas,[9] Daniel R. Carvalho,[10] Heiko Bratke,[11] Marte Gjøl Haug,[12] Jennifer B. Phillips,[4] Jeremy Wegner,[4] Michael Tiemeyer,[13] Kazuhiro Aoki,[13] Undiagnosed Diseases Network, Scottish Genome Partnership, Ann Nordgren,[7,14] Anna Hammarsjö,[7,14] Angela L. Duker,[15] Luis Rohena,[16,17] Hanne Buciek Hove,[18] Jakob Ek,[19] David Adams,[6] Cynthia J. Tifft,[6] Tito Onyekweli,[6] Tara Weixel,[6] Ellen Macnamara,[6] Kelly Radtke,[20] Zöe Powis,[20] Dawn Earl,[21] Melissa Gabriel,[22] Alvaro H. Serrano Russi,[22] Lauren Brick,[23] Mariya Kozenko,[23] Emma Tham,[7,14] Kimiyo M. Raymond,[8] John A. Phillips III,[24] George E. Tiller,[25] William G. Wilson,[26] Rizwan Hamid,[24] May C.V. Malicdan,[6] Gen Nishimura,[27,28] Giedre Grigelioniene,[7,14] Andrew Jackson,[5,30] Monte Westerfield,[4,30] Michael B. Bober,[15,30] William A. Gahl,[6,30] and Hudson H. Freeze[3,30]

The conserved oligomeric Golgi (COG) complex is involved in intracellular vesicular transport, and is composed of eight subunits distributed in two lobes, lobe A (COG1-4) and lobe B (COG5-8). We describe fourteen individuals with Saul-Wilson syndrome, a rare form of primordial dwarfism with characteristic facial and radiographic features. All affected subjects harbored heterozygous *de novo* variants in *COG4*, giving rise to the same recurrent amino acid substitution (p.Gly516Arg). Affected individuals' fibroblasts, whose COG4 mRNA and protein were not decreased, exhibited delayed anterograde vesicular trafficking from the ER to the Golgi and accelerated retrograde vesicular recycling from the Golgi to the ER. This altered steady-state equilibrium led to a decrease in Golgi volume, as well as morphologic abnormalities with collapse of the Golgi stacks. Despite these abnormalities of the Golgi apparatus, protein glycosylation in sera and fibroblasts from affected subjects was not notably altered, but decorin, a proteoglycan secreted into the extracellular matrix, showed altered Golgi-dependent glycosylation. In summary, we define a specific heterozygous COG4 substitution as the molecular basis of Saul-Wilson syndrome, a rare skeletal dysplasia distinct from biallelic COG4-CDG.

Introduction

Saul-Wilson syndrome (SWS) is a rare skeletal dysplasia with characteristic dysmorphic and radiographic findings, as well as early developmental delay, primarily involving speech, with eventual normal cognition. Clinical findings include marked short stature, prominent forehead with an enlarged anterior fontanel, prominent eyes with cataracts, narrow nasal bridge with a convex nasal ridge, micrognathia, clubfoot, brachydactyly, and short distal phalanges of fingers. Radiographic changes include platyspondyly, irregular end plates of vertebral bodies, and hypoplasia of the odontoid process with cervical instability in the spine, coxa valga, overtubulation, metaphyseal flaring

[1]Medical Genetics Branch, National Human Genome Research Institute, National Institutes of Health, Bethesda, MD 20892, USA; [2]Division of Genetics and Metabolism, Children's National Health System, Washington, DC 20010, USA; [3]Human Genetics Program, Sanford Burnham Prebys Medical Discovery Institute, La Jolla, CA 92037, USA; [4]Institute of Neuroscience, University of Oregon, Eugene, OR 97403, USA; [5]MRC Human Genetics Unit, Institute of Genetics and Molecular Medicine, University of Edinburgh, Edinburgh EH4 2XU, UK; [6]Office of the Clinical Director, National Human Genome Research Institute, National Institutes of Health, Bethesda, MD 20892, USA; [7]Department of Molecular Medicine and Surgery, Center for Molecular Medicine, Karolinska Institutet, 17176 Stockholm, Sweden; [8]Biochemical Genetics Laboratory, Mayo Clinic College of Medicine, Rochester, MN 55905, USA; [9]GeneDx, Gaithersburg, MD 20877, USA; [10]Genetic Unit, SARAH Network of Rehabilitation Hospitals, Brasília-DF, 70335-901, Brazil; [11]Department of Internal Medicine, Section of Paediatrics, Haugesund District Hospital, Fonna Health Trust, 5527 Haugesund, Norway; [12]Department of Medical Genetics, St. Olav's Hospital, 7006 Trondheim, Norway; [13]Complex Carbohydrate Research Center, University of Georgia, Athens, GA 30602, USA; [14]Department of Clinical Genetics, Karolinska University Hospital, 17176 Stockholm, Sweden; [15]Division of Orthogenetics, A.I. duPont Hospital for Children, Wilmington, DE, 19803, USA; [16]Division of Genetics, Department of Pediatrics, San Antonio Military Medical Center, San Antonio, TX, 78234, USA; [17]Department of Pediatrics, University of Texas Health Science Center, San Antonio, TX, 78229, USA; [18]Section of Rare Disorders, Department of Pediatrics, Rigshospitalet, 2100 Copenhagen, Denmark; [19]Department of Clinical Genetics, Rigshospitalet, 2100 Copenhagen, Denmark; [20]Ambry Genetics, Aliso Viejo, CA 92656, USA; [21]Division of Genetic Medicine, Seattle Children's, Seattle, WA, 98105, USA; [22]Division of Medical Genetics, Children's Hospital of Los Angeles, University of Southern California, Los Angeles, CA 90027, USA; [23]Division of Genetics, Department of Pediatrics, McMaster Children's Hospital, McMaster University, Hamilton Ontario L8S 4J9, Canada; [24]Division of Medical genetics and Genomic Medicine, Department of Pediatrics, Vanderbilt University Medical Center, Nashville, TN, 37232, USA; [25]Department of Genetics, Kaiser Permanente, Los Angeles, CA 90027, USA; [26]Department of Pediatrics, University of Virginia Health System, Charlottesville, VA 20903, USA; [27]Laboratory for Bone and Joint Diseases, RIKEN Center for Integrative Medical Sciences, Tokyo 108-8639, Japan; [28]Center for Intractable Diseases, Saitama Medical University Hospital, Saitama 350-0495, Japan
[29]These authors contributed equally to this work
[30]These authors contributed equally to this work
*Correspondence: carlos.ferreira@nih.gov
https://doi.org/10.1016/j.ajhg.2018.09.003.

and megaepiphyses in the long bones, while the hands and feet exhibit short phalanges, metacarpals and metatarsals, cone-shaped epiphyses of phalanges, and accessory ossification centers of metacarpals and metatarsals. Since its original description in 1990 as a provisionally new skeletal dysplasia, only five cases have been reported,[1–3] all from different families. Some essential characteristics of SWS (i.e., severe pre-and postnatal growth retardation with possible microcephaly and skeletal dysplasia) can fall within the category of microcephalic osteodysplastic primordial dwarfism.[4,5] In fact, a prior nosology of genetic skeletal disorders included SWS in the same group of slender bone dysplasias that contained microcephalic osteodysplastic primordial dwarfism type II (MOPDII, OMIM 210720).[6] However, due to the uncertainty about the etiology and identity of SWS as a genetic disorder, it was excluded from the two subsequent nosologies[7,8] and, due to its rarity, it is not included as a discrete entity in the Online Mendelian Inheritance in Man (OMIM) catalog.

Here we present fourteen individuals with SWS and a recurrent *de novo* heterozygous variant in *COG4* (MIM: 606976, NM_015386.2:c.1546G>A, or c.1546G>C/p.Gly516Arg), a component of the Complex Oligomeric Golgi (COG) trafficking complex. The COG complex controls retrograde and anterograde vesicular protein trafficking and is composed of eight subunits distributed in two lobes, lobe A (COG1-4), and lobe B (COG5-8).[9] The COG complex interacts with various other proteins involved in vesicular trafficking, including SNARES, SNARE-interacting proteins, Rab GTPases, coiled-coil tethers, and COPI coat proteins.[10] Our description of the basic molecular defect in SWS expands the phenotypic spectrum of the disease and helps elucidate the cellular pathogenesis of this rare skeletal dysplasia.

Material and Methods

Subjects

Individual P1.1 was initially seen at Vanderbilt Children's Hospital and enrolled under protocol 15-HG-0130, "Clinical and Genetic Evaluation of Individuals With Undiagnosed Disorders Through the Undiagnosed Diseases Network."[11–13] Upon further clinical analysis at the National Institutes of Health Clinical Center this subject was enrolled in protocol 14-HG-0071 "Clinical and Basic Investigations into Known and Suspected Congenital Disorders of Glycosylation." Individuals P2.1 and P7.1 were also enrolled in protocol 14-HG-0071. Individuals P3.1, P4.1, P5.1, P6.1, P9.1, P10.1, P11.1, P12.1, and P13.1 were enrolled in protocol 76-HG-0238, "Diagnosis and Treatment of Patients with Inborn Errors of Metabolism or Other Genetic Disorders." The aforementioned protocols were approved by the National Human Genome Research Institute (NHGRI) Institutional Review Board (IRB).

Individuals P3.1, P4.1, and P8.1 were enrolled in research protocol "Enquiry of participation in a research project about clinical and molecular studies on rare congenital skeletal disorders," approved by the IRB of the Karolinska Institute in Sweden (2014/983-31/1). Individuals P2.1, P5.1, P5.2, and P7.1 were enrolled in the Primordial Registry at Nemours/Alfred I. duPont Hospital for Children, approved by the Nemours IRB, and sequencing of individuals P2.1 and P7.1 was approved by the Scottish Multicenter Research Ethics Committee (04:MRE00/19). Individuals P5.1, P5.2, P6.1, P9.1, P10.1, P11.1, and P12.1 underwent sequencing on a clinical basis. Written consent was obtained from all affected individuals or their parents.

Fibroblast Cultures

From a forearm skin punch biopsy, primary dermal fibroblasts were cultured from individuals P1.1, P2.1, P3.1, P4.1, P5.1, P7.1, P9.1, and P12.1; age- and gender-matched control cell lines were obtained from Coriell Institute for Medical Research (Camden, NJ, USA) and American Type Culture Collection (ATCC, Manassas, VA, USA). Fibroblasts were cultured in Dulbecco's Modified Eagle's medium (DMEM) containing 1 g/L glucose (4.5 g/L for mRNA expression, co-immunoprecipitation, and Golgi morphology experiments) supplemented with 10% heat inactivated fetal bovine serum and 1% antibiotic-antimycotic (Life Technologies, Carlsbad, CA, USA).

Genetic Analysis

Different technologies and analysis pipelines were used for subjects sequenced by seven different institutions; details are presented in the Supplemental Experimental Procedures section.

mRNA Expression Analysis

Total RNA was extracted from frozen fibroblast pellets using a Maxwell RSC instrument with the corresponding simplyRNA Cells Kit (Promega, Madison, WI, USA) following the manufacturers protocol with DNase1 treatment. Two μg of RNA was reverse transcribed using the Omniscript Reverse Transcriptase kit (QIAGEN, Valencia, CA, USA). Quantitative RT-PCR was performed on an Applied Biosystems 7500 Fast Real-Time PCR System (Life Technologies, Grand Island, NY, USA) using a TaqMan gene-expression mastermix and the following TaqMan assays: COG1 (Hs00372622_m1), COG2 (Hs00201197_m1), COG3 (Hs00230134_m1), COG4 (Hs01094456_m1), COG5 (Hs00197140_m1), COG6 (Hs01037401_m1), COG7 (Hs00411394_m1) and COG8 (Hs00260744_m1). Expression was normalized using GAPDH (Hs02758991_g1) and POLR2A (Hs00172187_m1) as endogenous controls.

Protein Level Analysis

For analysis of COG4, cells were harvested using SDS lysis buffer (62.5 mM Tris-HCl, pH 6.8, 2% SDS, and 10% glycerol) supplemented with protease and phosphatase inhibitors (Sigma-Aldrich, St. Louis, MO, USA). Lysates were sonicated and heated at 95°C for 5 min followed by centrifugation at 10,000 rpm for 5 min. Equivalent amounts of total lysates were then fractionated on a 4%–15% polyacrylamide gel and transferred to a nitrocellulose membrane using the Transblot Turbo transfer system (Bio-Rad, Hercules, CA, USA). The membrane was blocked with Odyssey TBS Blocking buffer (LI-COR, Lincoln, NE, USA) and probed with anti-COG4 antibody produced in rabbit (A305-555A, Bethyl Laboratories, Montgomery, TX, USA) and anti-Vinculin antibody produced in mouse (V9131, Sigma Aldrich, St. Louis, MO, USA). Secondary antibodies Donkey anti-rabbit IRDye 680RD and Donkey anti-mouse IRDye 800CW (LI-COR, Lincoln, NE, USA) were applied and imaging was done using a 9140 Odyssey CLx infrared imaging system with Image Studio software for analysis (LI-COR, Lincoln, NE, USA).

For analysis of other COG subunits, human fibroblast cells were harvested by SDS lysis buffer as previously described.[14] The lysates (10 μg of protein) obtained from each cell line were fractionated by SDS-PAGE on 8% gels and immunoblotted with rabbit polyclonal COG subunit antibodies (COG antibodies provided by Dr. Daniel Ungar, University of York, UK). The blots were developed using a SuperSignal West Dura enhanced chemiluminescence kit (ThermoFisher Scientific, Waltham, MA, USA) according to the manufacturer's instructions, and quantified by ImageJ (National Institutes of Health, Bethesda, MD, USA).

Golgi Morphology by Immunofluorescence

For analysis of Golgi morphology, fibroblasts were seeded at 0.5×10^5 per 12-mm round coverslip. After an overnight incubation at 37°C, the cells were fixed with 4% paraformaldehyde in PBS and permeabilized with 0.5% NP-40 in PBS. Coverslips were incubated for 1 h with 4% bovine serum albumin (BSA) in PBS and probed with anti-GM130 produced in mouse (BD Biosciences, Franklin Lakes, NJ, USA) and anti-TGN46 produced in sheep (Genetex, Irvine, CA, USA) overnight at 4°C. After washing in PBS, they were incubated for 1 hr with secondary Alexa Fluor-555 donkey anti-mouse IgG and Alexa Fluor-488 donkey anti-sheep IgG (Life Technologies, Grand Island, NY, USA), co-stained with Hoescht 33342 and mounted using ProLong Gold Antifade Mountant (Life Technologies, Carlsbad, CA, USA). Z stacked images were obtained using a Zeiss LSM700 confocal laser-scanning microscope with a 63× oil-based objective and a 20× objective and Images were processed with LSM software ZEN Black 2012 software (Carl Zeiss Microscopy GmbH, Jena, Germany).

Golgi Three-Dimensional Rendering and Volumetric Analysis

Alexa Fluor 488 anti-Giantin antibodies (BioLegend, San Diego, CA, USA) were used as a marker of the Golgi. All fibroblast Z series reconstructions were imaged with a pinhole size of 1 Airy Unit and a Z-step interval of 0.2 μm at 4x magnification. LSM Z series files of the Golgi were opened in Imaris software (Bitplane, South Windsor, CT, USA) as volumes, and the surface of the Golgi was smoothened by setting the surface detail at 0.1 μm. Each Golgi isosurface was visually inspected to ensure that it closely followed the underlying original three-dimensional image and did not incorporate voxels outside of the observable Golgi region. Each isosurfaced Golgi was selected and its volume recorded.[15] The nucleus was stained with DAPI (GeneTex Inc., Alton Pkwy, Irvine, CA) and its volume measured as above; the surface detail was set at 1 μm.

Decorin Immunoblotting

For secreted decorin analysis, fibroblast cells were grown in normal condition for three days to reach ~80% confluency, then the medium was replaced with a serum-free formulation. After 4 days, the medium was collected and concentrated using Microcon centrifugal filter unit YM-10 columns (Millipore-Sigma, Darmstadt, Germany). For intracellular decorin analysis, cells were lysed in 0.1M Tris-Cl pH 8.0 buffer with protease inhibitor cocktail (Roche, Mannheim, Germany) followed by sonication. The concentrated medium and cell lysate from fibroblast cultures were subjected to SDS–PAGE using 6 or 8% SDS polyacrylamide gels. Separated proteins were transferred to a PVDF membrane and decorin was detected with anti-human decorin antibody (clone 115402; R&D Systems, Minneapolis, MN, USA).

Brefeldin A-Induced Transport Assays

For the brefeldin A (BFA)-induced retrograde transport assay, fibroblasts from two controls and four subjects were grown on glass coverslips for two days. After removal of the medium, cells were incubated with prewarmed normal growth medium containing 0.25 μg/ml BFA for 0, 7.5, 15, 22.5, 30 and 45 min at 23°C. The incubations were stopped by washing cells with DPBS and cells were fixed with 4% paraformaldehyde for 10 min at room temperature. Cells were permeabilized and stained by immunofluorescence using Alexa Fluor 488 anti-Giantin antibodies (BioLegend, San Diego, CA, USA). The percentage of cells with ER staining was determined at the given time points. Images were obtained using an Olympus IX71 microscope (Olympus Corporation, Tokyo, Japan), and processed by MetaMorph software (Molecular Devices, San Jose, CA, USA). Between 80 to 100 cells were counted in replicate samples for each time point. A similar assay was performed using TGN46 (a marker of the trans-Golgi network) instead of Giantin (a cis- and medial-Golgi marker) antibodies. Primary antibody was anti-TGN46 produced in sheep (Genetex, Irvine, CA, USA) while secondary antibodies were Alexa Fluor-488 donkey anti-sheep IgG (Life Technologies, Grand Island, NY, USA).

For the anterograde transport assay, fibroblasts from two unaffected controls, four subjects, and a positive control obtained from an individual with biallelic variants in *COG8*[16] were grown on glass coverslips for 2 days. After incubating the cells with 0.25 μg/ml brefeldin A for 1 hr at 37°C, cells were washed with DPBS twice, then switched to new plates with prewarmed normal growth medium and incubated for 0, 20, 30, 40, 60, 80, 100, and 120 min at 37°C. The incubations were stopped and processed as described above.

Zebrafish Maintenance and Staging

Wild-type ABCxTu, *cog4*^{b1311}, *cog4*^{b1312}, and transgenic *Tg [p7.2sox10:mRFP]*^{vu234} adult zebrafish[17] were maintained as previously described.[18] Embryos and larvae were staged according to the standard staging series.[19] All zebrafish procedures were approved by the University of Oregon Institutional Animal Care and Use Committee (IACUC).

Zebrafish Immunolabeling, *In Situ* Hybridization, Phalloidin Staining, and Alcian Blue Staining

Whole-mount larvae were labeled following previously published protocols[20] with minor modifications. Five dpf larvae were fixed in BT fixative overnight and permeabilized in 2.5% Tween-20 for 18 hr. Primary antibodies were rabbit anti-Cog4 (Novus Biologicals, Littleton, CO, USA; 1:500), mouse anti-Collagen type II (Developmental Studies Hybridoma Bank, Iowa City, IA, USA; II-II6B3, 1:200), and mouse anti-GM130 (BD Transduction Laboratories, 1:500). Secondary antibodies were biotinylated horse anti-rabbit and biotinylated horse anti-mouse (Vector Laboratories, Burlingame, CA, USA; 1:500). The procedure for the *in situ* hybridization followed previously published protocols.[20] Larvae were hybridized with a digoxigenin-labeled RNA probe spanning a 736 bp coding sequence between exons 3 and 8 of *cog4*. Stained larvae were embedded in 1% agarose, 0.5% agar, 5% sucrose medium, and 16 μm cryosections were cut. Zebrafish

RNA probe for *collagen I alpha2* (*col1a2*) was kindly provided by Dr. John H. Postlethwait. Phalloidin staining was performed as previously described.[21] Alcian blue staining was performed as previously described.[22]

Generation of Indel Mutant Alleles using CRISPR

Two single guide RNAs (sgRNA) were designed that contained targeting sequences in exon 4 (5′-GGCTGTACCAAGCGATTC AG-3′) and exon 12 (5′-GCTCTGCAGGACCTGCAGCG-3′) of *cog4*, respectively. sgRNA and *cas9* RNAs were co-injected at the 1-cell stage. Indel mutations were identified using the following primers: targeted sequence in exon 4: forward 5′- TGGCAGAAAATGTCAG CAGC-3′ and reverse: 5′-GCAAAGGTAACCCTACTCGC-3′; targeted sequence in exon 12: forward: 5′-ACTCATAAGTTGCCAAT CTAGT-3′ and reverse: 5′-CTGGATGCTCACCAAGTATG-3′.

Zebrafish Imaging

Differential interference contrast images of the inner ear and images of Alcian blue stained ceratohyal cartilages were acquired using a Zeiss Axioplan2 compound microscope. Images of immunolabeled cells and larvae were acquired using a Zeiss LSM 5 confocal microscope. Images were analyzed using ImageJ (National Institutes of Health, Bethesda, MD, USA).

Statistical Analysis

For Golgi morphology count, a chi-square test was performed using R[23] (script accessible in Supplemental Experimental Procedures). For quantification of fibroblasts' glycan peak intensities, multiple t tests were performed (one per row), with correction for multiple comparisons performed via the Holm-Sidak method, alpha = 5.0%, using Prism 6.0c (Graphpad Software Inc, La Jolla, CA, USA). For other statistical analyses, an unpaired Student's t test was performed with Excel (Microsoft Corporation, Redmond, WA, USA). Statistical significance was assigned to a two-tailed p value < 0.05.

Results

Clinical Features

The clinical and imaging characteristics of fourteen individuals with SWS are summarized in Table 1. Individuals P2.1 and P12.1 were previously reported as two of the original probands with SWS (P12.1 corresponds to subject 2 in the original description of the syndrome by Saul and Wilson,[1] whereas P2.1 corresponds to subject 1 in Hersh et al.[2]). Affected newborns are born small for gestational age, have extreme short stature postnatally, and often have microcephaly, leading to a differential diagnosis within the microcephalic primordial dwarfism spectrum. Hearing loss appears to be another canonical feature of the disease. Representative clinical photos from subjects of different ages are shown in Figure 1, whereas characteristic radiographic findings are shown in Figure S1.

A Recurrent Heterozygous Substitution in COG4 Causes Saul-Wilson Syndrome

All subjects harbored one of two possible *COG4* variants, c.1546G>A or c.1546G>C (GenBank: NM_015386.2). Both variants give rise to an identical *de novo* heterozygous amino acid substitution, p.Gly516Arg (NP_056201.2).

Compared to control cells, fibroblasts from affected individuals showed normal mRNA expression (Figure 2A), and protein level of COG4 (Figure 2B) and other COG subunits (not shown) was not decreased, confirming that the variant leads to production of a stable protein. Protein modeling predicts the loss of a loop structure in the mutant protein (Figure S2). However, binding of COG4 to other COG subunits was not altered (Figure S3).

Altered Golgi Morphology and Volume

Because the COG4 protein is part of a large COG complex that governs membrane movement between the Golgi and ER, we examined the morphology and total volume of the Golgi in fibroblasts obtained from individuals with SWS. Golgi morphology was significantly altered in fibroblasts of three tested subjects, with only 51.1% (n = 237, P1.1), 52.8% (n = 254, P4.1), and 54.9% (n = 268, P5.1) of the Golgi complexes exhibiting normal morphology in contrast to 93.9% (n = 214, GM01582) in control fibroblasts (Figures 3A and 3B, Figure S4). Abnormal Golgi morphology was defined as co-localization of GM130 and TGN46, suggesting collapse of the cis- and trans-Golgi stacks. The Golgi volume in affected subject cells was significantly decreased compared to that of unaffected cells ($p < 0.0001$), since the volume in controls averaged 491 μm^3 based on staining with Giantin, a Golgi membrane marker; cells from affected individuals averaged 109 μm^3 (Figure 3C). The nuclear volume was also decreased (1,158 μm^3 in controls, 729 μm^3 in cells from affected subjects, $p = 0.0016$). After normalizing to nuclear volume, the volume of the Golgi in cells from affected individuals was 2.8-fold lower compared to that in control cells ($p = 0.0005$).

Protein glycosylation occurs in the Golgi apparatus. Nevertheless, despite the marked reduction in Golgi volume within cells from subjects, glycan analysis in the mutant fibroblasts (Figure S5) and serum/plasma (Figure S6), as well as glycosylation status of serum transferrin and apoCIII (not shown), were not measurably different from that of controls.

The initiation and polymerization of glycosaminoglycans (GAG) onto its core protein (i.e., the glycosylation of proteoglycans) also takes place mainly in the Golgi apparatus. More than 98% of decorin was secreted by fibroblasts to the extracellular matrix (data not shown). Extracellular decorin from affected individuals showed a greater proportion of higher molecular weight components compared to control cells (Figure 4A). Similarly, intracellular decorin in affected individuals exhibited a clear upward shift of the bands containing GAG chains (Figure 4B). Finally, a smaller proportion of intracellular decorin contained extended GAG chains in affected individuals when compared to controls (Figure 4C).

Table 1. Clinical, Imaging and Molecular Features of Individuals with Saul-Wilson Syndrome

	P1.1	P2.1	P3.1	P4.1	P5.1	P5.2	P6.1	P7.1	P8.1	P9.1	P10.1	P11.1	P12.1	P13.1
Gender	M	F	M	F	M	M	M	F	M	F	M	F	M	F
Geographic origin	Am	Am	Ger	Brz	Am	Am	Am	Am	Swe	Can	Dan	Hisp	Am	Kor
Age at last examination	4 y 4 m	29 y	6 y 9 m	7 y 4 m	8 y 0 m	3 y 10 m	9 y 0 m	27 y	9 m	9 y	10 y 8 m	18 m	39 y	3 y 2 m
Growth Parameters														
Birth weight in kg (*Z* score[a])	2.2 (−2.2)	2.52 (−1.7)	1.85 (−2.7)	1.45 (−3.8)	2.24 (−2.1)	1.75 (−2.9)	2.18 (−2.2)	1.96 (−2.8)	2.8 (−1.2)	2.13 (−2.5)	2.78 (−1.3)	1.81 (−3.1)	1.5 (−3.3)	2.15 (−2.4)
Birth length in cm (*Z* score[a])	43.1 (−2.6)	48 (−0.7)	44 (−2.3)	38 (−5.1)	48.3 (−0.7)	41 (−3.4)	45.5 (−1.7)	ND	46 (−1.6)	39 (−4.7)	49 (−0.4)	42 (−3.3)	ND	45 (−2.0)
Birth OFC in cm (*Z* score[a])	32.7 (−1.4)	32 (−1.9)	30 (−2.6)	29 (−3.9)	33 (−1.3)	31.5 (−1.9)	30.5 (−2.4)	ND	33.5 (−1.1)	30.5 (−2.9)	34 (−0.8)	ND	ND	32 (−1.9)
Current weight in kg (*Z* score[a])	9.7 (−4.2)	25.3 (−4.8)	9.8 (−5.0)	9.5 (−4.9)	14.5 (−3.7)	9.25 (−4.3)	21.3 (−2.0)	27.2 (−4.5)	5.76 (−3.8)	24.6 (−1.1)	16 (−3.9)	5.15 (−5.8)	39 (−3.6)	7.7 (−4.6)
Current height in cm (*Z* score[a])	80.9 (−5.4)	109.7 (−8.3)	86.2 (−6.4)	82 (−7.7)	93.4 (−6.0)	78 (−5.6)	107 (−4.3)	107.1 (−8.7)	62.5 (−3.5)	109 (−4.0)	105 (−5.4)	59.5 (−6.3)	106 (−9.8)	71 (−6.2)
Current OFC in cm (*Z* score[a])	48.4 (−1.5)	49 (−5.0)	46.5 (−4.0)	48.5 (−2.4)	50.6 (−1.2)	51.2 (+0.6)	50 (−1.9)	51.4 (−2.7)	46.2 (+0.8)	51 (−0.7)	51 (−1.5)	43.5 (−2.6)	ND	48.5 (−0.2)
Craniofacial Features														
Progeroid appearance	+	+	+	+	−	−	+	−	−	+	+	+	−	−
Prominent forehead	+	+	+	+	+	+	+	+	+	+	+	+	+	+
AF enlargement or closure delay	+	+	+	+	ND	+	+	ND	+	+	+	+	+	+
Narrow nasal bridge	+	+	−	+	+	−	+	−	−	−	+	+	+	−
Convex nasal ridge	−	+	+	+	−	−	+	−	−	−	−	+	+	−
Micrognathia	+	+	+	+	−	−	+	+	+	+	+	+	+	+
Prominent veins	+	+	+	+	visible	Visible	+	visible	+	+	+	+	+	+
Ophthalmic Features														
Blue sclerae	+	+	−	+	−	−	−	+	−	−	+	+	+	+
Prominent eyes	+	+	+	+	+	+	+	+	+	+	+	+	+	−

(*Continued on next page*)

Table 1. ***Continued***

	P1.1	P2.1	P3.1	P4.1	P5.1	P5.2	P6.1	P7.1	P8.1	P9.1	P10.1	P11.1	P12.1	P13.1
Cataracts	+	+	+	+	+	+	+	+	–	+	+	ND	+	–
Retinal involvement[b]	+	+	-	+	–	ND	ND	+	ND	+	+	ND	ND	–
Audiologic Features														
Hearing loss	BL SNHL[c]	BL SNHL	–	BL mixed	BL cond	Cond	BL cond	+	–	–	+	+	+	BL cond
Hematologic Features														
Neutropenia	–	+	+	+	+	+	+	+	–	–	+	+	+	+
Development														
Speech delay	+	+	+	+	ND	ND	+	+	ND	–	–	+	+	–
Motor delay	+	+	+	+	+	+	–	+	+	–	+	+	+	+
Skeletal Features														
Pectus	+	+	–	+	–	–	–	+	–	–	–	–	+	–
Clubfoot	+	+	–	+	+	–	+	–	+	–	+	+	+	+
Short distal ph	+	+	+	+	+	+	+	+	–	+	+	–	+	+
Radiographic Features														
Overtubulation of long bones	+	+	+	+	+	+	+	+	+	+	+	ND	+	+
Metaphyseal long bone flaring	+	+	+	+ (mild)	+ (mild)	+	+	+	+	+	+	ND	+	+
Megaepiphyses	+	+	+	+	+	+	+	+	+	+	+	ND	+	+
Coxa valga	+	+	+	+	+	+	+	+	+	+	+	ND	+	+
Dysplastic proximal radius	+	+	+	+	+	+	+	–	+	–	+	ND	ND	+
Madelung-like deformity of wrist	–	+	–	+[d]	+[d]	–	–	+	–	+	–	ND	–	–
Shortening of proximal fibula	+	+	+ (mild)	–	+ (mild)	+	+	ND	+	–	+	ND	ND	+
Premature DJD	–[e]	+	–[e]	–[e]	–[e]	–[e]	–[e]	+	–[e]	–[e]	–[e]	ND	+	–[e]
Platyspondyly	+	+[f]	–	+[f]	+[f]	–	–	–	+	–	+	ND	–	+
Irregular vertebral endplates	+ (mild)	+	–	+[g]	+[g]	–	+	+	+ (mild)	+ (mild)	+	ND	+	+ (mild)

(*Continued on next page*)

Table 1. ***Continued***

	P1.1	P2.1	P3.1	P4.1	P5.1	P5.2	P6.1	P7.1	P8.1	P9.1	P10.1	P11.1	P12.1	P13.1
Hypoplasia of T12 or L1	–	+	–	+	+	+	+	+	–	–	–	ND	+	–
Dens hypoplasia	+	+	+	+	+	+	+	+	+	+	+	ND	+	+
Subluxed C1-C2	–	–	+	–	–	–	–	+	–	–	+	ND	–	–
Platybasia	+	+	ND	+	+	+	+	+	–	+	+	ND	ND	–
Short mt/mc/ph	+	+	+	+	+	+	+	+	+	+	+	ND	+	+
Cone-shaped epiphyses of ph	+	+	+	+	+	+	+	ND	+	+	+	ND	+	+
Ivory epiphyses of ph	+	+	–	+	+	–[e]	+	ND	–[e]	+	+	ND	+	–[e]
Pseudoepiphyses of mc	+	+	+	+	+	+	+	ND	–[e]	+	+	ND	+	+
Neuroimaging Features														
Ventriculomegaly	+	ND	–	–	+[h]	ND	+	ND	ND	–	+[h]	+	ND	–
SC compression	+	+	–	+	–	ND	ND	ND	ND	–	–	ND	ND	ND
SC syrinx	ND	+	ND	–	ND	ND	ND	ND	ND	–	–	ND	ND	ND
Molecular Findings														
cDNA change (NM_015386.2)	c.1546G>A	c.1546G>A	c.1546G>A	c.1546G>C	c.1546G>A	c.1546G>A	c.1546G>A	c.1546G>A	c.1546G>A	c.1546G>A	c.1546G>A	c.1546G>A	c.1546G>C	c.1546G>C
Protein change (NP_056201.2)	p.Gly516Arg													

Abbreviations: AF, anterior fontanelle; Am, American; BL, bilateral; Brz, Brazilian; Can, Canadian; cond, conductive; Dan, Danish; DJD, degenerative joint disease; F, female; Ger, German; Hisp, Hispanic; IAC, internal auditory canal; Kor, Korean; M, male; mc, metacarpals; mt, metatarsals; ND, not described; HL, hearing loss; OFC, occipitofrontal circumference; ph, phalanges; SC, spinal cord; SNHL, sensorineural hearing loss; Swe, Swedish.[a]*Z* scores calculated using 2000 Centers for Disease Control and Prevention (CDC) growth charts.
[b]Retinal pigmentary changes or night blindness.
[c]Failed newborn hearing screen; temporal bone CT at 4 months of age showed dysplastic cochlea, dilated and bulbous internal auditory canals, and mildly dilated vestibules and semicircular canals.
[d]Mild; manifests with age.
[e]Too young to assess.
[f]At younger age; become tall vertebrae with age.
[g]At older age.
[h]Hydrocephalus.

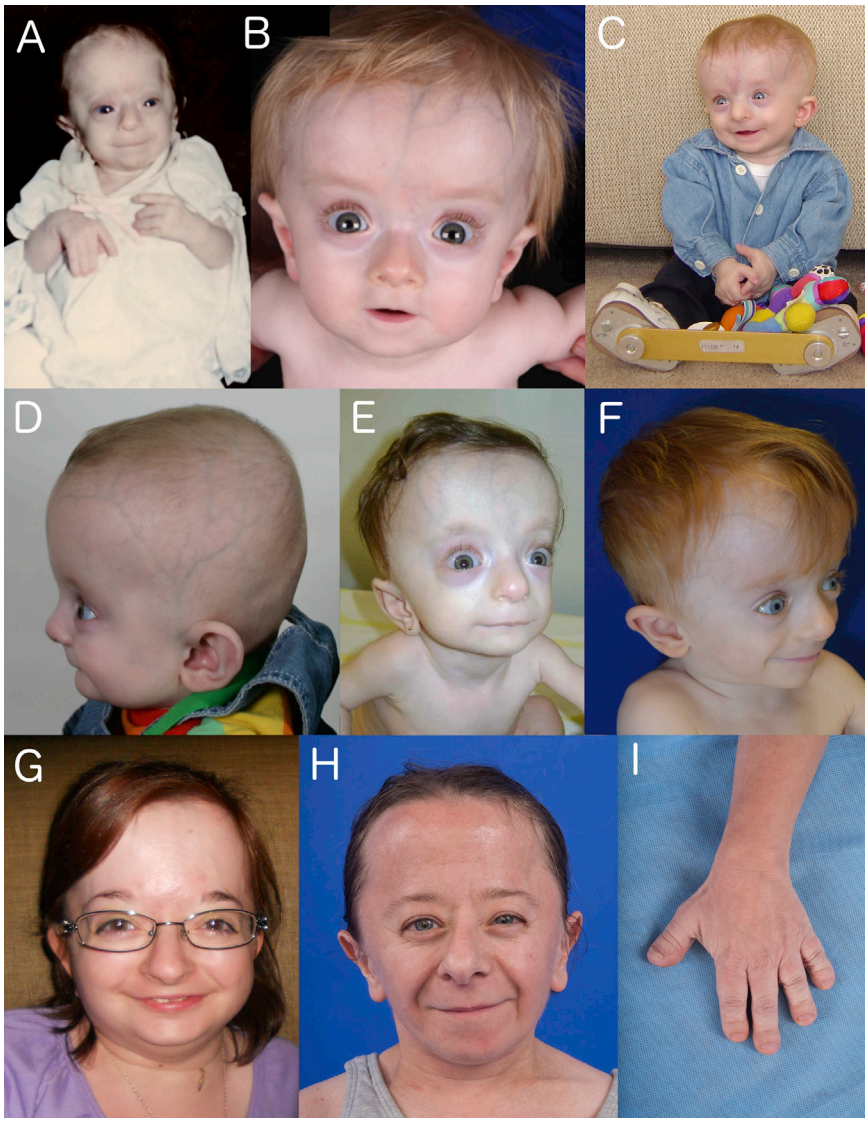

Figure 1. Clinical Features of Individuals with Saul-Wilson Syndrome
(A) P2.1 as an infant, showing a progeroid appearance, sparse eyebrows, and thin vermillion of the upper lip.
(B) P8.1 at 6 months of age, showing prominent forehead, veins, and eyes, thin vermilion of the upper lip, and micrognathia.
(C) P6.1 at 7 months of age, showing a progeroid appearance, relative macrocephaly, prominent forehead and veins, sparse eyebrows, low-set ears, low hanging columella, thin vermillion of the upper lip, and use of boots and bar orthosis as therapy for clubfoot.
(D) P10.1 at 7 months of age, showing prominent scalp veins and low-set ears.
(E) P4.1 at 1 year of age, showing relative macrocephaly, prominent forehead, veins and eyes, sparse eyebrows, low hanging columella, and thin vermillion of the upper and lower lips.
(F) P1.1 at 4 years of age, showing prominent forehead, veins, and eyes, and thin vermillion of the upper and lower lips.
(G) P7.1 at 20 years of age, showing prominent forehead, sparse eyebrows, narrow nasal bridge, low hanging columella, and thin vermillion of the upper lip.
(H) P2.1 at 29 years of age, showing prominent forehead, sparse eyebrows, narrow nasal bridge, low hanging columella, and thin vermillion of the upper and lower lips.
(I) P2.1 at 29 years of age, showing telebrachydactyly.

Brefeldin A-Induced Protein Transport Is Impaired

Brefeldin A (BFA) is an inhibitor of the vesicle membrane trafficking mediated by the coat protein complex, COPI. Such trafficking is involved in the process of Golgi-to-ER retrograde transport,[24,25] in which the COG complex functions; hence BFA is widely used to examine the phenotype of human COG mutant cells. We treated control and affected subject fibroblasts with 0.25 μg/ml BFA at room temperature and recorded the increase in the ER-localized staining of Giantin over time. In previous studies using cells from individuals with biallelic variants in a single COG subunit, cells showed a delayed response to BFA treatment.[14,16,26–28] Surprisingly, the BFA-induced retrograde transport was significantly faster in affected subject cells compared to controls (Figure 5A). In contrast, when BFA was washed out and the Golgi allowed to reform, the anterograde transport was slower in cells from affected subjects compared to controls (Figure 5B).

The trans-Golgi network (TGN) is a tubular-reticular structure adjacent to the trans-Golgi cisternae, acting as a protein sorting station with a role both in protein secretion and endocytosis.[29] BFA is known to produce effects in Golgi cisternae different from those in the TGN.[30] In particular, BFA is known to alter the kinetics of recycling between the plasma membrane and the TGN.[31] After BFA treatment, TGN46 was distributed in the cytoplasm as small, membrane-bound structures. Although the rate of loss of TGN structure was difficult to quantify objectively, this TGN breakdown appeared slightly faster in affected cells than in control cells; this difference was seen mainly 30 min after treatment (Figure S7).

The Subcellular Localization of COG Subunits Is Unaltered

Fractionation assays by differential centrifugation showed that the subcellular distribution of COG4 is unaltered. The majority of COG4 is in the cytosolic fraction (supernatant fraction from 100,000 g spin or 100kgS) and less than 5% of COG4 is membrane-bound (large membrane pellet fraction from 15,000 g spin or 15kgP, and small membrane pellet fraction from 100,000 g spin or 100kgP) in control and subjects' cells (Figure S8). This is

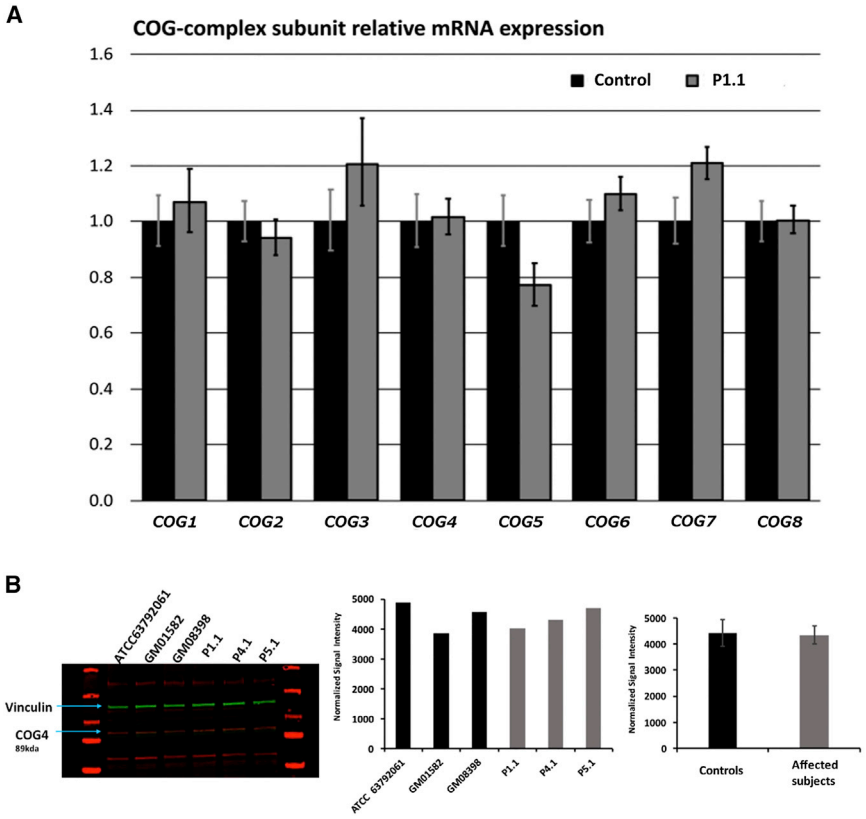

Figure 2. COG Subunit Expression

(A) mRNA expression of each of the COG-subunits in P1.1 (gray) compared to control (GM08398, black). No significant changes in expression were observed. Measurements were performed in quadruplicate. Error bars represent 95% confidence interval.

(B) Infrared fluorescent western blot analysis (left) of COG4 in three control (GM08398, GM01582 and ATCC63792061) and three affected subject (P1.1, P4.1 and P5.1) fibroblast lines. Vinculin served as a loading control and in the calculation of normalized signal intensity. Quantitative analysis showing normalized signal intensity of COG4 in individual samples (middle). Mean protein level of COG4 in affected subjects versus controls; error bars represent SD.

consistent with published data on COG4 distribution.[26] The cytosolic versus membrane-bound distribution of the other COG subunits was also similar in control and affected subject cells (Figure S8).

A Portion of COG4 Assembles into Larger Complexes

The COG complex comprises eight subunits and their association and dissociation is dynamic. Density gradient centrifugation is a sensitive method to separate different-sized complexes formed by COG subunits.[26] We observed the presence of two peaks of COG4 in the cytosolic fraction: the majority is present in fraction 4 in both control and subjects' cells (Figure S9) but there was a visible shift of approximately 13% of COG4 to heavier fractions in affected subject cells.

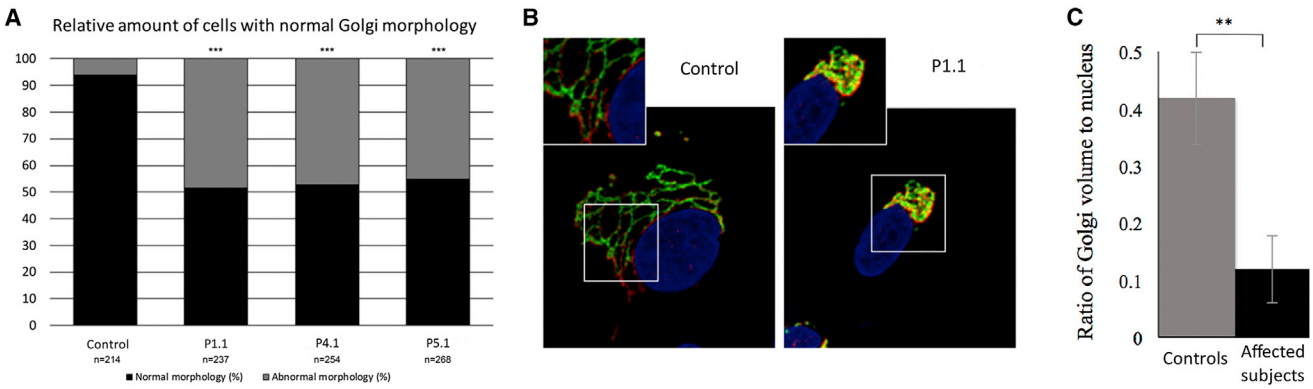

Figure 3. Golgi Morphology and Volumetric Analysis

(A) Compared to control fibroblasts (GM01582) that had normal Golgi morphology in 93.9% of the cells, P1.1, P4.1, and P5.1 only had normal morphology in 51.1%, 52.8%, and 54.9% of their cells, respectively. ***$p < 0.0005$ compared to the control. Affected subjects did not significantly differ from each other.

(B) Representative images of a Golgi with normal morphology in the control fibroblasts and a Golgi with abnormal morphology in P1.1 fibroblasts. Images were taken using the 63× oil-based objective. *Cis*-Golgi is stained with GM130 (red), trans-Golgi with TGN46 (green), and DNA with Hoescht 33342 (blue). The yellow signal in the affected subject cells represents co-localization of GM130 and TGN46, suggesting that the cis- and trans-Golgi are collapsed.

(C) The volumes of Giantin-labeled Golgi and DAPI-labeled nuclei were determined by Imaris software. A significant decrease in the ratio of Golgi-to-nucleus volume was seen in affected subject cell lines. Controls represent the average ratio for five cells from ATCC63792061 and GM8398 cell lines. Affected subjects represent the average ratio for 13 cells from P1.1, P4.1 and P5.1 cell lines. Error bars represent SD. **$p < 0.005$.

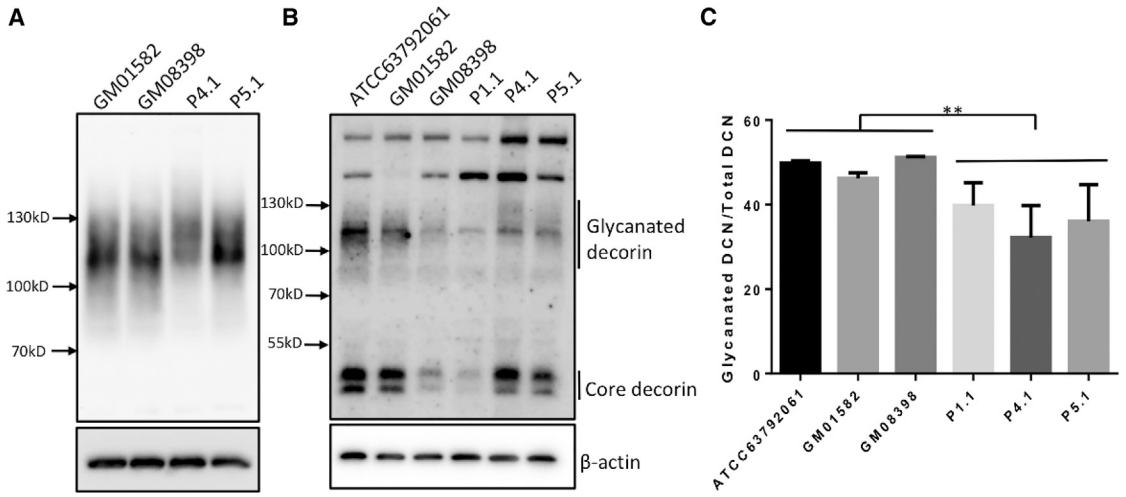

Figure 4. Decorin Immunoblotting in Control and Affected Individual Fibroblasts
(A) Western blot analysis of secreted decorin.
(B) Western blot analysis of intracellular decorin. The size ranges for the fully glycanated form of decorin and its core protein are indicated. A portion of decorin is extended with GAG chains (MW 100−130+kD), while a significant portion is not glycosylated and runs as a doublet at about 40kD.
(C) Levels of glycanated decorin were quantified against total decorin levels. The decorin bands between 70–150kD and core decorin bands (~40kD) in cell lysates were used to calculate the ratio of glycanated decorin to total decorin. Experiments were repeated in duplicate with similar results. Representative blots are shown. **$p < 0.005$.

The result indicates that a greater portion of COG4 exists in larger complexes.

Zebrafish *cog4*$^{-/-}$ Mutants Have Inner Ear, Growth, and Skeletal Defects

To establish the normal developmental functions of COG4, we used CRISPR/Cas9 gene editing to generate two mutant alleles of the zebrafish ortholog, *cog4* (Figure S10). Both mutations introduced frameshifts followed by premature stop codons, one in exon 4 (*cog4*^{b1311}, c.352_359del, p.I118Gfs*) and the other in exon 12 (*cog4*^{b1312}, c.1499_1511del, p.D500Gfs*6). We did not observe significant differences in the phenotypes of the two alleles. As in affected subject's fibroblasts, Golgi structure was disrupted in mutant cells (Figure S11), but unlike our observations from affected subjects' fibroblasts (Figure S5) and serum/plasma (Figure S6), we found defects in the processing of N- and O-linked glycans (Figure S12A-B), and decreased glycosphingolipid complexity (Figure S12C).

The inner ear was malformed in zebrafish mutants, with abnormally shaped semicircular canals (Figures 6A and 6B). Mechanosensory hair cells in the inner ear (Figures 6C–6D, G) and neuromasts (Figures 6E–6F, H) of mutants had reduced numbers of hair bundles. Response to auditory stimuli was greatly reduced in mutants (2% of 53 mutants responded, compared to 100% of 102 wild-types). Homozygous mutant animals were significantly shorter than wild-type ones (Figures 7A–7B, E; Z-score = −10.2). Mutants also had craniofacial defects (Figures 7A–7D) with a smaller jaw, smaller inner ears (Figures 7A–7B, F), slightly smaller eyes (Figures 7C and 7D), and stubby "clubbed" pectoral fins (Figures 7C and 7D). mRNA *in situ* hybridization showed that *cog4* is expressed in these

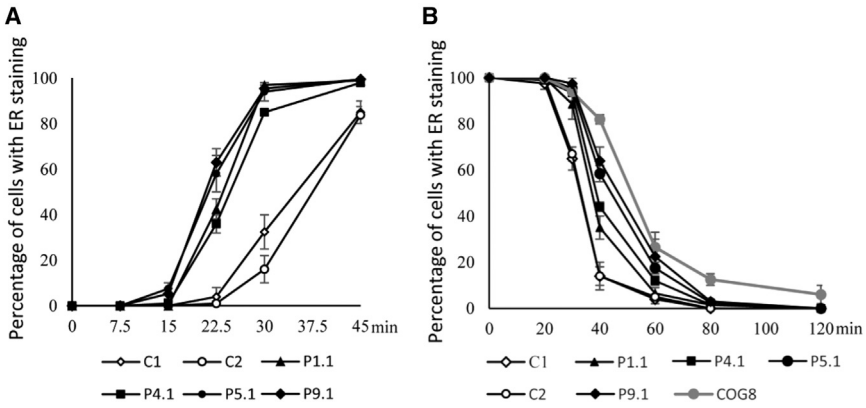

Figure 5. Brefeldin A Trafficking Assays
(A) BFA-induced retrograde transport kinetics of control and affected subject cells. Between 80 and 100 cells were counted for each time point. The experiment was performed in duplicate. C1, ATCC63792061; C2, GM08398.
(B) Golgi protein anterograde transport kinetics of control and affected subject cells was measured after treatment with BFA for 1 hr followed by washout (T = 0). Between 80 and 100 cells were counted for each time point. The experiment was performed in duplicate. C1, ATCC63792061; C2, GM08398; COG8, positive control. Error bars represent SD.

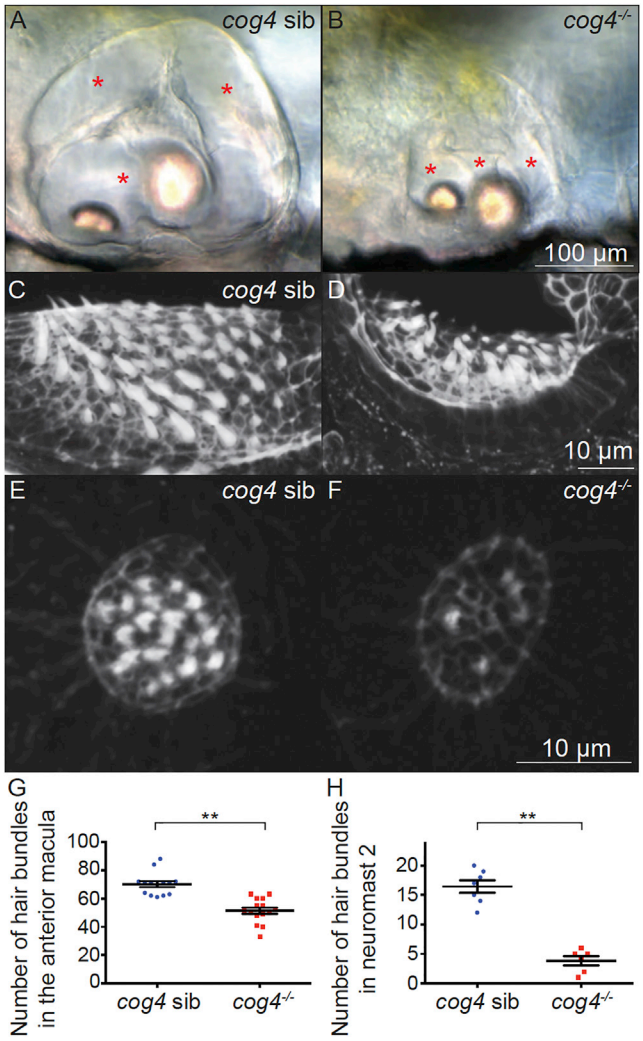

Figure 6. Morphogenesis and Function of the Inner Ear Are Abnormal in *cog4*-Deficient Zebrafish

(A and B) Morphology of the inner ear in *cog4* sibling (A) and $cog4^{-/-}$ mutant (B) larvae. Red stars indicate the semicircular canals.

(C–F) Phalloidin staining of the anterior macula in *cog4* sibling (C) and *cog4* mutant (D) larvae. Phalloidin staining of the second posterior neuromast in *cog4* sibling (E) and *cog4* mutant (F) larvae.

(G) Number of hair bundles in the anterior macula of *cog4* mutants (n = 15 larvae) and *cog4* siblings (n = 14 larvae).

(H) Number of hair bundles in the second posterior neuromast of *cog4* mutants (n = 6 larvae) and *cog4* siblings (n = 7 larvae). **$p < 0.01$. All data obtained at 5 dpf, anterior to the left (A–F).

structures (Figure S13), and immunohistochemistry showed that the protein is deficient in biallelic mutants (Figure S14). Reduced Alcian blue staining of the jaw in mutants indicated defects in proteoglycan secretion (Figures 7G and 7H), and *col1a2* expression was reduced in the fin (Figures 7I and 7J). Expression of collagen type II was normal in the jaw, however, suggesting that not all secreted proteins are affected by biallelic *cog4* mutations. Notably, chondrocytes did not stack properly (Figures 7K and 7L). Taken together, these findings establish a role for *cog4* in inner ear development and skeletogenesis, associated with defective Golgi structure.

Discussion

We show that a heterozygous *de novo* p.Gly516Arg COG4 variant is responsible for SWS, a rare skeletal dysplasia characterized by short stature, facial dysmorphisms, hearing loss, cataracts, developmental delay, and normal cognition. This is phenotypically distinct from the three reported individuals with classic, biallelic loss-of-function, or hypomorphic *COG4* mutations, who presented with seizures, hypotonia, intellectual disability, microcephaly, elevated transaminases, and, in one case, recurrent infections,[26,32–34] and from individuals with loss-of-function mutations in other COG subunits associated with congenital disorders of glycosylation (CDG). These distinct phenotypes and the recurrent nature of the p.Gly516Arg variant therefore suggest the SWS mutation to be gain-of-function. Supporting this notion, SWS cells have accelerated, rather than the delayed retrograde Golgi-to-ER transport seen in cells with biallelic *COG4* deficiency.[26,33] In addition, loss-of-function *COG4*-mutant cells have impaired glycosylation and reduced COG4 protein levels,[26] whereas SWS cells had no reduction in COG4 protein level, with apparently normal glycosylation in serum, plasma and fibroblasts.

In SWS cells, accelerated retrograde transport combines with delayed anterograde transport to disrupt the normal dynamics of Golgi trafficking, creating smaller Golgi volumes. Despite the strikingly abnormal architecture of the Golgi and its collapsed stacks in almost 50% of fibroblasts from individuals with SWS, and the expected maldistribution of proteins toward the ER and away from the Golgi, glycosylation analysis in serum appeared normal, in contrast to the altered serum glycosylation seen in individuals with COG4-CDG. One caveat is that the expression of lobe B subunits was unaltered; prior studies have shown that lobe B is essential for preventing retrograde trafficking of β1,4-galactosyltransferase 1 and α2,6-sialyltransferase 1.[35] Additionally, glycomic analysis of the eleven most abundant fibroblast N-glycans did not detect statistically significant differences between control (n = 2) and affected subject (n = 5) cells. However, a comprehensive analysis of processing defects in affected subject cells would require the quantification of a significantly expanded portfolio of N-glycans in order to fully assess precursor/product flux through multiple, specific glycan biosynthetic pathways. The limited glycomic profiles we have quantified in control and affected subject fibroblasts are not sufficient to report whether altered Golgi morphology impacts any particular N-glycan processing pathway. Furthermore, efforts to understand the impact of the SWS COG4 variant on cellular glycosylation may benefit from assessing glycosylation in cell types other than fibroblasts that are more reliant on specific glycosylation pathways.

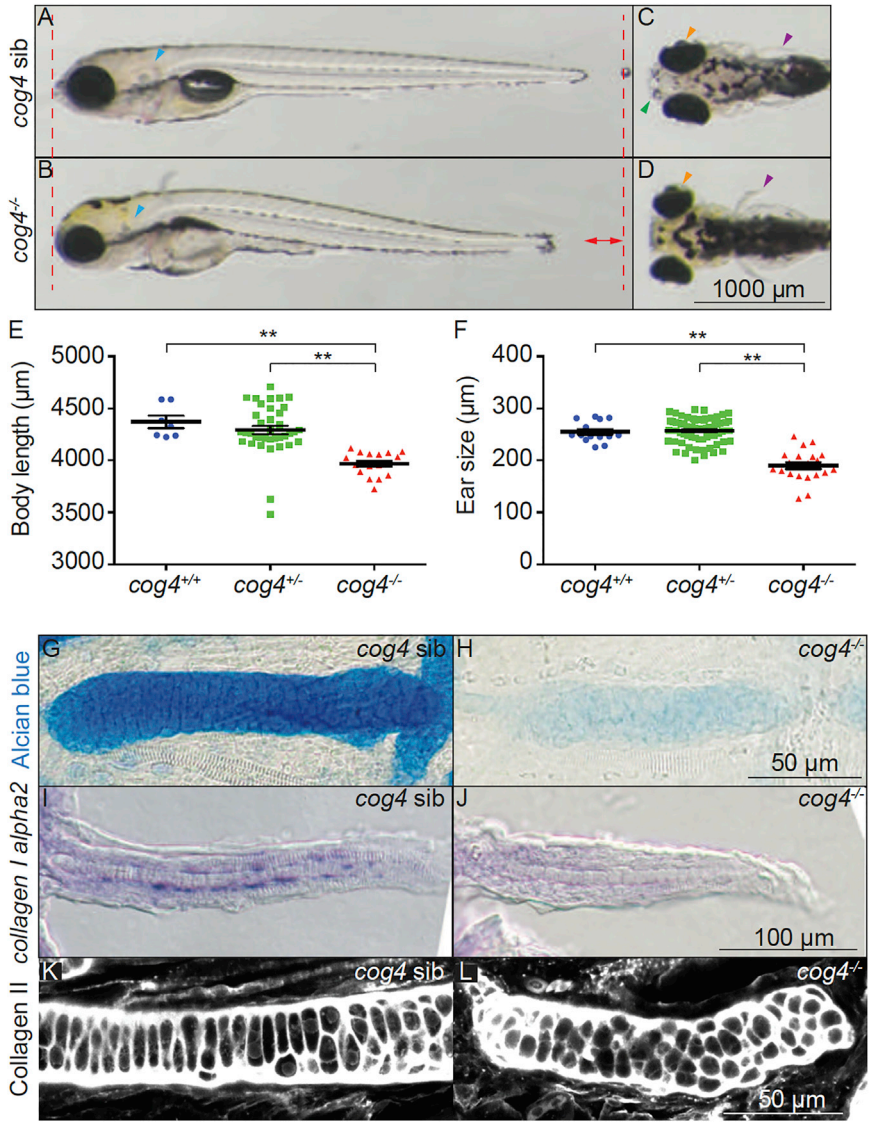

Figure 7. Zebrafish *cog4*-Deficient Mutants Have Morphological and Secretory Defects

(A and B) Lateral views of (A) *cog4* sibling and (B) biallelic $cog4^{-/-}$ mutant larvae. Red dashed lines indicate the anterior (jaw extension) and posterior (caudal fin) ends of the wild-type larvae. Red double arrow in B marks the length difference between wild-type and mutant larvae. Blue arrowheads indicate the inner ear.

(C and D) Dorsal views of *cog4* sibling (C) and $cog4^{-/-}$ mutant (D) larvae. Orange arrowheads indicate the eyes, and purple arrowheads the pectoral fins; green arrowhead indicates the forward extent of the jaw in (C).

(E) Body length in homozygous wild-type $cog4^{+/+}$ (n = 7 larvae), heterozygous $cog4^{+/-}$ (n = 37 larvae) and biallelic homozygous $cog4^{-/-}$ mutant larvae (n = 17 larvae). Length was measured as in (A).

(F) Inner ear size in $cog4^{+/+}$ (n = 14), $cog4^{+/-}$ (n = 70), and $cog4^{-/-}$ larvae (n = 21). Size was measured as distance along the antero-posterior axis of the inner ear. **$p < 0.01$.

(G and H) Alcian blue staining of the ceratohyal in *cog4* sibling (G) and biallelic mutant (H) larvae.

(I and J) *col1a2* mRNA *in situ* hybridization in the pectoral fin of *cog4* sibling (I) and mutant (J) larvae.

(K and L) Immunolabeling of collagen type II in the ceratohyal of *cog4* sibling (K) and mutant (L) larvae. All data obtained at 5 days postfertilization (dpf), anterior to the left (A–D, G–L).

Decorin is a widely-distributed extracellular matrix proteoglycan containing a single chondroitin sulfate (CS) or dermatan sulfate (DS) chain attached to serine residue 4.[36] We found decorin with a higher molecular weight both in media and inside fibroblasts from affected individuals. This could be due to longer GAG chain length, increased sulfation, or both. In addition, a smaller proportion of decorin is glycosylated with CS or DS. These results indicate that SWS affects at least two different aspects of decorin glycosylation, namely initiation, and polymerization or sulfation. Initiation of proteoglycan glycosylation takes place in early Golgi compartments (cis- and medial-Golgi), whereas polymerization and sulfation take place in late Golgi compartments (trans-Golgi and trans-Golgi network).[37,38] This suggests that multiple Golgi compartments are affected in SWS cells. It has been previously shown that the biosynthesis of GAG depends on intact inter-compartmental Golgi transport,[39] and that the COG complex is essential for normal intra-Golgi transport.[26] Our zebrafish data support the fact that COG4 is necessary for normal secretion of proteoglycans (Figures 7G and 7H), and establish that it is required for normal skeletogenesis and cartilage architecture.

Previous reports indicate that both decreased and increased COG4 protein levels lead to disrupted vesicular homeostasis. Prior experiments have demonstrated that doubling levels of COG4 protein in control cells via viral transduction led to abnormal retrograde trafficking,[26] and lentiviral complementation of wild-type COG4 in fibroblasts derived from individuals with COG4 deficiency failed to rescue the retrograde trafficking delay.[33] In contrast, increasing the levels of wild-type protein rescues the retrograde trafficking delay seen in fibroblasts from affected subjects with deficiencies of COG1,[40] COG5,[27] COG6,[28] COG7,[41] and COG8.[16] Thus, this COG4 dosage effect seems unique among COG complex proteins, and it is possible that the recurrent SWS mutation could mediate its effects via modulation of protein turnover. A comprehensive investigation of the impact of the SWS mutation on protein level and stability of COG4 and other lobe A subunits is currently being pursued.

One consequence of the recurrent COG4 substitution might be the formation of additional protein complexes. Human COG4 is known to interact with syntaxin 5, syntaxin 16, VTI1A, GOSR1, SCFD1, VPS45, RAB1A, RAB4A, RAB30, and VCP.[10] Size distribution studies in affected subject cell extracts showed that COG4 protein was present in high molecular weight complexes, in keeping with the formation of intact COG complexes. Indeed, higher molecular weight complexes appeared to be more frequent in SWS cells, potentially suggesting the recruitment of additional interacting protein(s), which if confirmed may provide a useful avenue for future investigations.

Whatever the cellular perturbations associated with the COG4 p.Gly516Arg variant, they result in the distinctive clinical phenotype of SWS, a skeletal dysplasia (Table 1). This is not the first example of a defect in vesicular trafficking altering skeletal homeostasis; other genetic defects cause variable phenotypes such as osteopetrosis[42] (MIM: 611497 and 615085) with increased bone mineral density, a syndromic form of osteogenesis imperfecta[43] (MIM: 616294) and geroderma osteodysplasticum[44] (MIM: 231070) with bone fragility, rhizomelic short stature with deficiency of a subnit of the coatamer 1 protein complex[45] (MIM: 617164), cranio-lenticulo-sutural dysplasia (MIM: 607812) with abnormal anterograde vesicular trafficking,[46] the lethal achondrogenesis type 1A[47] (MIM: 200600), and Dyggve-Melchior-Clausen (MIM: 223800) with spondyloepimetaphyseal changes and delayed anterograde and retrograde trafficking.[48] To that list, we now add a rare but likely underdiagnosed cause of primordial dwarfism, i.e., Saul-Wilson syndrome.

Supplemental Data

Supplemental Data include 14 figures and Supplemental Experimental Procedures and can be found with this article online at https://doi.org/10.1016/j.ajhg.2018.09.003.

Consortia

Members of the Undiagnosed Diseases Network include David R. Adams, Aaron Aday, Mercedes E. Alejandro, Patrick Allard, Euan A. Ashley, Mahshid S. Azamian, Carlos A. Bacino, Eva Baker, Ashok Balasubramanyam, Hayk Barseghyan, Gabriel F. Batzli, Alan H. Beggs, Babak Behnam, Hugo J. Bellen, Jonathan A. Bernstein, Gerard T. Berry, Anna Bican, David P. Bick, Camille L. Birch, Devon Bonner, Braden E. Boone, Bret L. Bostwick, Lauren C. Briere, Elly Brokamp, Donna M. Brown, Matthew Brush, Elizabeth A. Burke, Lindsay C. Burrage, Manish J. Butte, Shan Chen, Gary D. Clark, Terra R. Coakley, Joy D. Cogan, Heather A. Colley, Cynthia M. Cooper, Heidi Cope, William J. Craigen, Precilla D'Souza, Mariska Davids, Jean M. Davidson, Jyoti G. Dayal, Esteban C. Dell'Angelica, Shweta U. Dhar, Katrina M. Dipple, Laurel A. Donnell-Fink, Naghmeh Dorrani, Daniel C. Dorset, Emilie D. Douine, David D. Draper, Annika M. Dries, Laura Duncan, David J. Eckstein, Lisa T. Emrick, Christine M. Eng, Gregory M. Enns, Ascia Eskin, Cecilia Esteves, Tyra Estwick, Liliana Fernandez, Carlos R. Ferreira, Elizabeth L. Fieg, Paul G. Fisher, Brent L. Fogel, Noah D. Friedman, William A. Gahl, Emily Glanton, Rena A. Godfrey, Alica M. Goldman, David B. Goldstein, Sarah E. Gould, Jean-Philippe F. Gourdine, Catherine A. Groden, Andrea L. Gropman, Melissa Haendel, Rizwan Hamid, Neil A. Hanchard, Frances High, Ingrid A. Holm, Jason Hom, Ellen M. Howerton, Yong Huang, Fariha Jamal, Yong-hui Jiang, Jean M. Johnston, Angela L. Jones, Lefkothea Karaviti, David M. Koeller, Isaac S. Kohane, Jennefer N. Kohler, Donna M. Krasnewich, Susan Korrick, Mary Koziura, Joel B. Krier, Jennifer E. Kyle, Seema R. Lalani, C. Christopher Lau, Jozef Lazar, Kimberly LeBlanc, Brendan H. Lee, Hane Lee, Shawn E. Levy, Richard A. Lewis, Sharyn A. Lincoln, Sandra K. Loo, Joseph Loscalzo, Richard L. Maas, Ellen F. Macnamara, Calum A. MacRae, Valerie V. Maduro, Marta M. Majcherska, May Christine V. Malicdan, Laura A. Mamounas, Teri A. Manolio, Thomas C. Markello, Ronit Marom, Martin G. Martin, Julian A. Martínez-Agosto, Shruti Marwaha, Thomas May, Allyn McConkie-Rosell, Colleen E. McCormack, Alexa T. McCray, Jason D. Merker, Thomas O. Metz, Matthew Might, Paolo M. Moretti, Marie Morimoto, John J. Mulvihill, David R. Murdock, Jennifer L. Murphy, Donna M. Muzny, Michele E. Nehrebecky, Stan F. Nelson, J. Scott Newberry, John H. Newman, Sarah K. Nicholas, Donna Novacic, Jordan S. Orange, James P. Orengo, J. Carl Pallais, Christina GS. Palmer, Jeanette C. Papp, Neil H. Parker, Loren DM. Pena, John A. Phillips III, Jennifer E. Posey, John H. Postlethwait, Lorraine Potocki, Barbara N. Pusey, Genecee Renteria, Chloe M. Reuter, Lynette Rives, Amy K. Robertson, Lance H. Rodan, Jill A. Rosenfeld, Jacinda B. Sampson, Susan L. Samson, Kelly Schoch, Daryl A. Scott, Lisa Shakachite, Prashant Sharma, Vandana Shashi, Rebecca Signer, Edwin K. Silverman, Janet S. Sinsheimer, Kevin S. Smith, Rebecca C. Spillmann, Joan M. Stoler, Nicholas Stong, Jennifer A. Sullivan, David A. Sweetser, Queenie K.-G. Tan, Cynthia J. Tifft, Camilo Toro, Alyssa A. Tran, Tiina K. Urv, Eric Vilain, Tiphanie P. Vogel, Daryl M. Waggott, Colleen E. Wahl, Nicole M. Walley, Chris A. Walsh, Melissa Walker, Jijun Wan, Michael F. Wangler, Patricia A. Ward, Katrina M. Waters, Bobbie-Jo M. Webb-Robertson, Monte Westerfield, Matthew T. Wheeler, Anastasia L. Wise, Lynne A. Wolfe, Elizabeth A. Worthey, Shinya Yamamoto, John Yang, Yaping Yang, Amanda J. Yoon, Guoyun Yu, Diane B. Zastrow, Chunli Zhao, and Allison Zheng.

Members of the Scottish Genome Partnership include Timothy J. Aitman, Andrew V. Biankin, Susanna L. Cooke, Wendy Inglis Humphrey, Sancha Martin, Lynne Mennie, Alison Meynert, Zosia Miedzybrodzka, Fiona Murphy, Craig Nourse, Javier Santoyo-Lopez, Colin A. Semple, and Nicola Williams.

Acknowledgments

This work was supported by the Intramural Research Program of the NHGRI, as well as NIH U54 NS093793. The Freeze lab was supported by The Rocket Fund, NIH R01 DK99551, and HHSN268201700060P. The Stockholm team has received financial support through the regional agreement on medical training and clinical research (ALF) between Stockholm County Council and Karolinska Institutet, KID (Karolinska Institutet's Doctoral fellowship to AH), by grants from Kronprinsessan Lovisas and Axel Tiellmans Minnesfond, Barncancerfonden, Hjärnfonden, Samariten, Sällskapet Barnavård, Promobilia Foundations, and Stiftelsen Frimurare Barnhuset i Stockholm. The Jackson lab was supported by an ERC Starter Grant (281847), by a Medical Research Council Human Genetics Unit core grant (MRC, U127580972), and the Scottish Genomes Partnership. The Scottish Genomes Partnership is funded by the Chief Scientist Office of the Scottish Government Health Directorates [SGP/1] and The Medical Research Council Whole Genome Sequencing for Health and Wealth Initiative.

The Primordial Registry at Nemours/Alfred I. duPont Hospital is supported by the Potentials Foundation and the Walking With Giants Foundation. The zebrafish lab received support from NIH HD22486 in addition to the U54, and the zebrafish glycomic analysis was supported by NIH-NIGMS (P41 GM103490 to M.T.) and the NIH Common Fund (R21 AI129873 to K.A.). We especially thank the families for their participation in research throughout the world. Without their contribution, knowledge about these rare conditions would not be as robust as it currently is.

Declaration of Interests

B.D.S., M.T.C., and G.D. are employees of GeneDx, a division of OPKO Health, Inc.; B.D.S. has stock options in OPKO Health, Inc. Z.P. and K.R. are employees of Ambry Genetics.

Received: May 28, 2018
Accepted: August 31, 2018
Published: October 4, 2018

Web Resources

The URLs for data presented herein are as follows:
OMIM, http://www.omim.org/
R statistical software, https://www.r-project.org/
SWISS-MODEL, http://swissmodel.expasy.org/

References

1. Saul, R.A., and Wilson, W.G. (1990). A "new" skeletal dysplasia in two unrelated boys. Am. J. Med. Genet. *35*, 388–393.
2. Hersh, J.H., Joyce, M.R., Spranger, J., Goatley, E.C., Lachman, R.S., Bhatt, S., and Rimoin, D.L. (1994). Microcephalic osteodysplastic dysplasia. Am. J. Med. Genet. *51*, 194–199.
3. Chinen, Y., Kaneshi, T., Kamiya, T., Hata, K., Nishimura, G., and Kaname, T. (2015). Progressive hip joint subluxation in Saul-Wilson syndrome. Am. J. Med. Genet. A. *167A*, 2834–2838.
4. Hall, J.G., Flora, C., Scott, C.I., Jr., Pauli, R.M., and Tanaka, K.I. (2004). Majewski osteodysplastic primordial dwarfism type II (MOPD II): natural history and clinical findings. Am. J. Med. Genet. A. *130A*, 55–72.
5. Bober, M.B., and Jackson, A.P. (2017). Microcephalic Osteodysplastic Primordial Dwarfism, Type II: a Clinical Review. Curr. Osteoporos. Rep. *15*, 61–69.
6. Superti-Furga, A., and Unger, S. (2007). Nosology and classification of genetic skeletal disorders: 2006 revision. Am. J. Med. Genet. A. *143A*, 1–18.
7. Warman, M.L., Cormier-Daire, V., Hall, C., Krakow, D., Lachman, R., LeMerrer, M., Mortier, G., Mundlos, S., Nishimura, G., Rimoin, D.L., et al. (2011). Nosology and classification of genetic skeletal disorders: 2010 revision. Am. J. Med. Genet. A. *155A*, 943–968.
8. Bonafe, L., Cormier-Daire, V., Hall, C., Lachman, R., Mortier, G., Mundlos, S., Nishimura, G., Sangiorgi, L., Savarirayan, R., Sillence, D., et al. (2015). Nosology and classification of genetic skeletal disorders: 2015 revision. Am. J. Med. Genet. A. *167A*, 2869–2892.
9. Ungar, D., Oka, T., Brittle, E.E., Vasile, E., Lupashin, V.V., Chatterton, J.E., Heuser, J.E., Krieger, M., and Waters, M.G. (2002). Characterization of a mammalian Golgi-localized protein complex, COG, that is required for normal Golgi morphology and function. J. Cell Biol. *157*, 405–415.
10. Willett, R., Ungar, D., and Lupashin, V. (2013). The Golgi puppet master: COG complex at center stage of membrane trafficking interactions. Histochem. Cell Biol. *140*, 271–283.
11. Gahl, W.A., Wise, A.L., and Ashley, E.A. (2015). The Undiagnosed Diseases Network of the National Institutes of Health: A National Extension. JAMA *314*, 1797–1798.
12. Gahl, W.A., Mulvihill, J.J., Toro, C., Markello, T.C., Wise, A.L., Ramoni, R.B., Adams, D.R., Tifft, C.J.; and UDN (2016). The NIH Undiagnosed Diseases Program and Network: Applications to modern medicine. Mol. Genet. Metab. *117*, 393–400.
13. Ramoni, R.B., Mulvihill, J.J., Adams, D.R., Allard, P., Ashley, E.A., Bernstein, J.A., Gahl, W.A., Hamid, R., Loscalzo, J., McCray, A.T., et al.; Undiagnosed Diseases Network (2017). The Undiagnosed Diseases Network: Accelerating Discovery about Health and Disease. Am. J. Hum. Genet. *100*, 185–192.
14. Steet, R., and Kornfeld, S. (2006). COG-7-deficient Human Fibroblasts Exhibit Altered Recycling of Golgi Proteins. Mol. Biol. Cell *17*, 2312–2321.
15. Burman, J.L., Hamlin, J.N.R., and McPherson, P.S. (2010). Scyl1 regulates Golgi morphology. PLoS ONE *5*, e9537.
16. Kranz, C., Ng, B.G., Sun, L., Sharma, V., Eklund, E.A., Miura, Y., Ungar, D., Lupashin, V., Winkel, R.D., Cipollo, J.F., et al. (2007). COG8 deficiency causes new congenital disorder of glycosylation type IIh. Hum. Mol. Genet. *16*, 731–741.
17. Kirby, B.B., Takada, N., Latimer, A.J., Shin, J., Carney, T.J., Kelsh, R.N., and Appel, B. (2006). In vivo time-lapse imaging shows dynamic oligodendrocyte progenitor behavior during zebrafish development. Nat. Neurosci. *9*, 1506–1511.
18. Westerfield, M. (2007). The Zebrafish Book: A Guide for the Laboratory Use of Zebrafish (Danio rerio) (Eugene, OR: University of Oregon Press).
19. Kimmel, C.B., Ballard, W.W., Kimmel, S.R., Ullmann, B., and Schilling, T.F. (1995). Stages of embryonic development of the zebrafish. Dev. Dyn. *203*, 253–310.
20. Thisse, C., and Thisse, B. (2008). High-resolution in situ hybridization to whole-mount zebrafish embryos. Nat. Protoc. *3*, 59–69.
21. Blanco-Sánchez, B., Clément, A., Fierro, J., Jr., Washbourne, P., and Westerfield, M. (2014). Complexes of Usher proteins preassemble at the endoplasmic reticulum and are required for trafficking and ER homeostasis. Dis. Model. Mech. *7*, 547–559.
22. Walker, M.B., and Kimmel, C.B. (2007). A two-color acid-free cartilage and bone stain for zebrafish larvae. Biotech. Histochem. *82*, 23–28.
23. R Core Team (2017). R: A language and environment for statistical computing (Vienna, Austria: R Foundation for Statistical Computing).
24. Lippincott-Schwartz, J., Yuan, L.C., Bonifacino, J.S., and Klausner, R.D. (1989). Rapid redistribution of Golgi proteins into the ER in cells treated with brefeldin A: evidence for membrane cycling from Golgi to ER. Cell *56*, 801–813.
25. Lippincott-Schwartz, J., Donaldson, J.G., Schweizer, A., Berger, E.G., Hauri, H.P., Yuan, L.C., and Klausner, R.D. (1990). Microtubule-dependent retrograde transport of proteins into the ER in the presence of brefeldin A suggests an ER recycling pathway. Cell *60*, 821–836.
26. Reynders, E., Foulquier, F., Leão Teles, E., Quelhas, D., Morelle, W., Rabouille, C., Annaert, W., and Matthijs, G. (2009). Golgi function and dysfunction in the first COG4-deficient CDG type II patient. Hum. Mol. Genet. *18*, 3244–3256.
27. Paesold-Burda, P., Maag, C., Troxler, H., Foulquier, F., Kleinert, P., Schnabel, S., Baumgartner, M., and Hennet, T. (2009).

Deficiency in COG5 causes a moderate form of congenital disorders of glycosylation. Hum. Mol. Genet. *18*, 4350–4356.
28. Lübbehusen, J., Thiel, C., Rind, N., Ungar, D., Prinsen, B.H.C.M.T., de Koning, T.J., van Hasselt, P.M., and Körner, C. (2010). Fatal outcome due to deficiency of subunit 6 of the conserved oligomeric Golgi complex leading to a new type of congenital disorders of glycosylation. Hum. Mol. Genet. *19*, 3623–3633.
29. Gu, F., Crump, C.M., and Thomas, G. (2001). Trans-Golgi network sorting. Cell. Mol. Life Sci. *58*, 1067–1084.
30. Ladinsky, M.S., and Howell, K.E. (1992). The trans-Golgi network can be dissected structurally and functionally from the cisternae of the Golgi complex by brefeldin A. Eur. J. Cell Biol. *59*, 92–105.
31. Reaves, B., Horn, M., and Banting, G. (1993). TGN38/41 recycles between the cell surface and the TGN: brefeldin A affects its rate of return to the TGN. Mol. Biol. Cell *4*, 93–105.
32. Miura, Y., Tay, S.K.H., Aw, M.M., Eklund, E.A., and Freeze, H.H. (2005). Clinical and biochemical characterization of a patient with congenital disorder of glycosylation (CDG) IIx. J. Pediatr. *147*, 851–853.
33. Ng, B.G., Sharma, V., Sun, L., Loh, E., Hong, W., Tay, S.K.H., and Freeze, H.H. (2011). Identification of the first COG-CDG patient of Indian origin. Mol. Genet. Metab. *102*, 364–367.
34. Felipe Rucián, A., Macaya Ruiz, A., del Toro Riera, M., and Girós, M. (2017). Severe infantile acute encephalopathy and COG4 mutation: CDG IIJ. Eur. J. Paediatr. Neurol. *21*, e140.
35. Peanne, R., Legrand, D., Duvet, S., Mir, A.-M., Matthijs, G., Rohrer, J., and Foulquier, F. (2011). Differential effects of lobe A and lobe B of the Conserved Oligomeric Golgi complex on the stability of beta1,4-galactosyltransferase 1 and alpha2,6-sialyltransferase 1. Glycobiology *21*, 864–876.
36. Chopra, R.K., Pearson, C.H., Pringle, G.A., Fackre, D.S., and Scott, P.G. (1985). Dermatan sulphate is located on serine-4 of bovine skin proteodermatan sulphate. Demonstration that most molecules possess only one glycosaminoglycan chain and comparison of amino acid sequences around glycosylation sites in different proteoglycans. Biochem. J. *232*, 277–279.
37. Silbert, J.E., and Sugumaran, G. (1995). Intracellular membranes in the synthesis, transport, and metabolism of proteoglycans. Biochim. Biophys. Acta *1241*, 371–384.
38. Uyama, T., Kitagawa, H., and Sugahara, K. (2007). 3.05 - Biosynthesis of Glycosaminoglycans and Proteoglycans. In Comprehensive Glycoscience, H. Kamerling, ed. (Oxford: Elsevier), pp. 79–104.
39. Fernández, C.J., and Warren, G. (1998). In vitro synthesis of sulfated glycosaminoglycans coupled to inter-compartmental Golgi transport. J. Biol. Chem. *273*, 19030–19039.
40. Foulquier, F., Vasile, E., Schollen, E., Callewaert, N., Raemaekers, T., Quelhas, D., Jaeken, J., Mills, P., Winchester, B., Krieger, M., et al. (2006). Conserved oligomeric Golgi complex subunit 1 deficiency reveals a previously uncharacterized congenital disorder of glycosylation type II. Proc. Natl. Acad. Sci. USA *103*, 3764–3769.
41. Wu, X., Steet, R.A., Bohorov, O., Bakker, J., Newell, J., Krieger, M., Spaapen, L., Kornfeld, S., and Freeze, H.H. (2004). Mutation of the COG complex subunit gene COG7 causes a lethal congenital disorder. Nat. Med. *10*, 518–523.
42. Stenbeck, G., and Coxon, F.P. (2014). Role of vesicular trafficking in skeletal dynamics. Curr. Opin. Pharmacol. *16*, 7–14.
43. Garbes, L., Kim, K., Rieß, A., Hoyer-Kuhn, H., Beleggia, F., Bevot, A., Kim, M.J., Huh, Y.H., Kweon, H.-S., Savarirayan, R., et al. (2015). Mutations in SEC24D, encoding a component of the COPII machinery, cause a syndromic form of osteogenesis imperfecta. Am. J. Hum. Genet. *96*, 432–439.
44. Hennies, H.C., Kornak, U., Zhang, H., Egerer, J., Zhang, X., Seifert, W., Kühnisch, J., Budde, B., Nätebus, M., Brancati, F., et al. (2008). Gerodermia osteodysplastica is caused by mutations in SCYL1BP1, a Rab-6 interacting golgin. Nat. Genet. *40*, 1410–1412.
45. Izumi, K., Brett, M., Nishi, E., Drunat, S., Tan, E.-S., Fujiki, K., Lebon, S., Cham, B., Masuda, K., Arakawa, M., et al. (2016). ARCN1 Mutations Cause a Recognizable Craniofacial Syndrome Due to COPI-Mediated Transport Defects. Am. J. Hum. Genet. *99*, 451–459.
46. Boyadjiev, S.A., Fromme, J.C., Ben, J., Chong, S.S., Nauta, C., Hur, D.J., Zhang, G., Hamamoto, S., Schekman, R., Ravazzola, M., et al. (2006). Cranio-lenticulo-sutural dysplasia is caused by a SEC23A mutation leading to abnormal endoplasmic-reticulum-to-Golgi trafficking. Nat. Genet. *38*, 1192–1197.
47. Smits, P., Bolton, A.D., Funari, V., Hong, M., Boyden, E.D., Lu, L., Manning, D.K., Dwyer, N.D., Moran, J.L., Prysak, M., et al. (2010). Lethal skeletal dysplasia in mice and humans lacking the golgin GMAP-210. N. Engl. J. Med. *362*, 206–216.
48. Osipovich, A.B., Jennings, J.L., Lin, Q., Link, A.J., and Ruley, H.E. (2008). Dyggve-Melchior-Clausen syndrome: chondrodysplasia resulting from defects in intracellular vesicle traffic. Proc. Natl. Acad. Sci. USA *105*, 16171–16176.